24th COBEM - 2017

24th ABCM International Congress of Mechanical Engineering
December 3-8, 2017, Curitiba, PR, Brazil

COBEM-2017-0723
STRUCTURAL BEHAVIOR OF CO-BONDED COMPOSITE STRUCTURES SUBJECT TO MODE I AND MODE II FATIGUE INDUCED DELAMINATION

F.P.Garpelli, F.M.González, N.N.A.Nale, M.A.Arbelo, M.V.Donadon
Instituto Tecnológico de Aeronáutica – ITA, São José dos Campos, SP, Brazil
felipegarpelli92@yahoo.com.br, francismgonzalezr@gmail.com, nubianale@gmail.com, marbelo@ita.br, donadon@ita.br

R.C.M.Sales
Faculdade de Tecnologia de São José dos campos – FATEC, São José dos Campos, SP, Brazil
rita.sales@fatec.sp.gov.br

M.Y.Shiino
Universidade Estadual Paulista (Unesp), Instituto de Ciência e Tecnologia, São José dos Campos, SP, Brazil
marcos.shiino@ict.unesp.br

H.B.Resende
Instituto de Pesquisas Tecnológicas – IPT, São José dos Campos, SP, Brazil
hresende@ipt.br

Abstract. *This research work describes an experimental study on the structural behavior of composite bonded joints subjected to Mode I and Mode II fatigue induced delamination. Mode I and Mode II fatigue tests were carried out using Double Cantilever Beam (DCB) and three-point bending End-Notched Flexure (3-ENF) specimens, respectively. Using this set up, the authors aimed to obtain the strain energy release rate (G) versus number of cycles (N_f) of crack initiation curve, which provides information about the delamination resistance of bonded joints composite materials under cyclic loading. The G/G_c ratios for Mode I and Mode II fatigue tests were defined based on closed form solutions for the DCB and 3-ENF testing configurations. In addition, quasi-static tests were also performed in order to characterize the critical strain energy release rates (G_{IC} and G_{IIC}) for Modes I and II delamination. The results from all tests showed an enhanced fatigue life performance of composite co-bonded joints in comparison with conventional co-cured joints. Additional scanning electron microscopy (SEM) images were made in the samples to certify that for the values of no-growth G, found experimentally, the crack tip did not present the delamination of the material, as expected.*

Keywords: *Fatigue Delamination, End notched Flexure, Double Cantilever Beam, No-Growth Onset Delamination.*

1. INTRODUCTION

The laminate is the most common form in which composite materials are used in aerostructures. The properties that can be emphasized are strength, stiffness and low weight. However, there are some problems such as delaminations, particularly under cyclic loadings (ASTM D6115, 2004).

Characterization of interlaminar toughness in Modes I and II (Maillet *et al.*, 2015; Al-Khudairi *et al*, 2015) is one of the first steps required in the development of robust design methodologies for damage tolerant composite lightweight structures, particularly in the design of complex structural components made of different parts, such as stiffened composite panels.

For joining composite parts, adhesives can provide specific benefits over other joining methods (Loh *et al*, 2002). Adhesive bonding process can simplify the plies assembly, increases production and quality, reduces production costs, enhances the strength to weight ratios and improves fatigue behavior (Sarado *et al*, 2016). Between these bonding processes, the co-bonding process is characterized when an uncured laminate is bonded to a cured laminate and they are cured afterwards, while in the co-curing process both laminates are cured together in a single processing operation without additional adhesive interface. The main objective of this work is to evaluate the structural behavior of composite co-bonded joints subject to Modes I and II fatigue induced delamination.

The testing configurations employed for Mode I and Mode II interlaminar fatigue tests are: double cantilever beam (DCB), 3-point-End notched flexure (3-ENF) and 4-point-End notched flexure (Hojo *et al*, 2006; O'Brien *et al*, 2010). The DCB fatigue tests were based on the ASTM standard (ASTM D6115, 2004), however there is no standard for Mode II. Based on the open literature (Davidson *et al*, 2007; Carreras *et al*, 2017; Sun and Davidson, 2006), DCB and 3-ENF configuration were chosen. The testing methodology proposed by O'Brien *et al.* (2010) was used as a procedure in order to obtain the G-N_f curve.

2. EXPERIMENTAL PROCEDURE

Mode I and Mode II fatigue tests are being performed on unidirectional carbon-epoxy co-bonding laminates (T800 fibers embedded in a 3900-2C toray prepeg UD) with a $[0^o]_{26}$ layup with a Teflon® film insert in the midplane, used as a crack starter. The sample's adhesive film is LOCTITE® EA9695. It is important to emphasize that thermoplastic particles were present at the interfaces in order to improve fracture toughness, these particles were highlighted via SEM in the in Odagiri *et al*. (1996) research. Dimensions of the specimens are showed in Fig. 1. The tests were performed at room temperature (RTA).

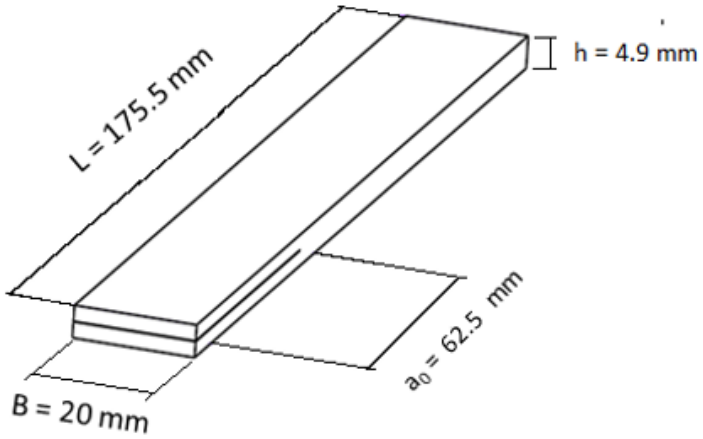

Figure 1: Dimensions of the specimens in millimeters.

2.1 Mode I Fatigue Tests

The tests have been carried out at the structures laboratory of the Aeronautics Institute of Technology – ITA using a servo-hydraulic Landmark test machine (type MTS 370.10) with a 100-lb load cell. This work is being used $N_a^{5\%}$ (decrease 5% in the maximum cyclic load) as an evidence of crack initiation or 10^6 cycles without decreasing 5% of the maximum cyclic load. The DCB test setup is shown in Fig. 2.

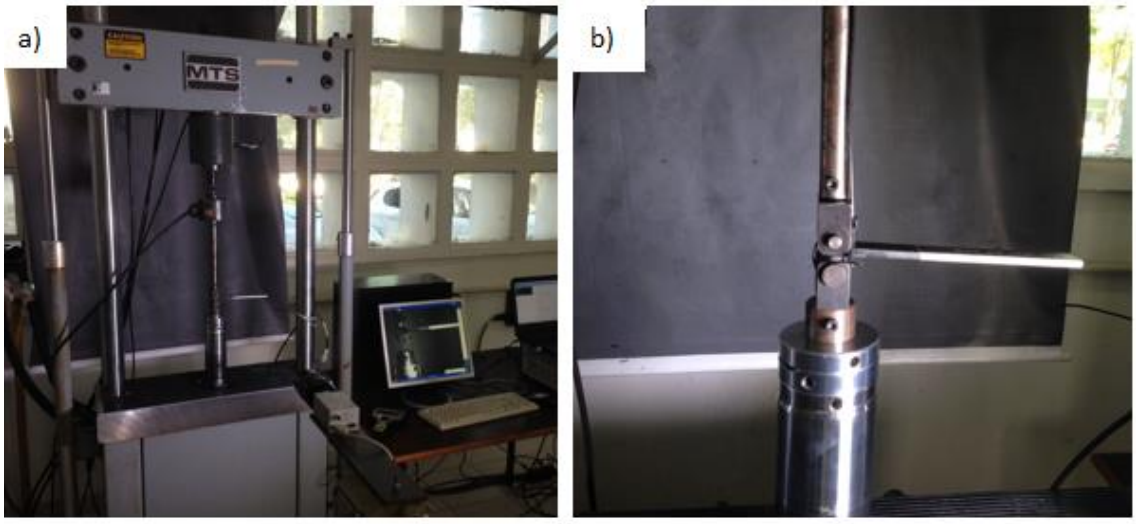

Figure 2: Fatigue Mode I test: a) DCB test setup and b) Sample details.

The average values of critical strain energy release rate (SERR) G_{Ic} ($[G_{Ic}]_{av}$), the modulus of elasticity (E), the average value of the critical load point and critical displacement for delamination growth, ($[\delta cr]_{av}$), were obtained from previous quasi-static tests (Brito *et al.*, 2016). Based on ASTM D6115 (2004) the maximum cyclic displacement is obtained from Eq. (1).

$$\frac{\delta_{\max}^{\ 2}}{\left[\delta_{cr}\right]_{av}^{\ 2}} = \frac{G_{IMax}}{G_{Ic}} \tag{1}$$

The tests have been carried out under displacement control defined in terms of sinusoidal function with ratio of $R = \delta_{max}/\delta_{min} = 0.1$ at a frequency of 5Hz. Various values of G_{Imax} must be set to obtain the curve G-N_f. From the values of δ_{max}, P_{max}, a at N = 1 and the averaged compliance constant Δ_{av} (from the quasi-static tests) the G_{Imax} for each testing condition is obtained by using Eq. (2).

$$G_{\mathrm{Im}ax} = \frac{3P_{\max}\delta_{\max}}{2B\left(a + \left|\Delta\right|_{av}\right)} \tag{2}$$

2.2 Mode II Fatigue Tests

An analytical model was implemented using MATLAB to predict the behavior of 3-ENF sample and to define the fatigue test parameters. The Eq. (3). and Eq. (4). represent the relationship between load and displacement in the middle of the beam, before and after delamination propagation, respectively (Donadon and Faria, 2016).

$$\delta = \frac{P\left(2L^3 + 3a_0^{\ 3}\right)}{12EI} \qquad Linear \tag{3}$$

$$\delta = \frac{P}{12EI}\left(2L^3 + \frac{\left(8G_{II}BEI\right)^{\frac{3}{2}}}{\sqrt{3}P^3}\right) \qquad \left(a < L\right) \tag{4}$$

where L is the half distance between lower points, δ is the central deflection, I is the specimen cross-sectional moment of inertia, a_0 is crack size (30 mm), B is the width (20 mm) and G_{II} is the Mode II SEER.

The 3-ENF fatigue tests have been performed on a servo-hydraulic test machine (MTS370.10) with a 15 kN load cell available at the LEL/IPT, according to the setup depicted in Fig. 3. The tests have been performed in a frequency of 5 Hz, R-ratio ($R= \delta_{max}/\delta_{min}=0.1$), applying a preload (10 N) to hold the sample in the test device (ASTM D7905, 2014) as shown in Fig. 3 and Fig. 4. The criterion adopted for stopping the test for a given G_{IImax} was the same defined in the previous section ($N_a^{5\%}$).

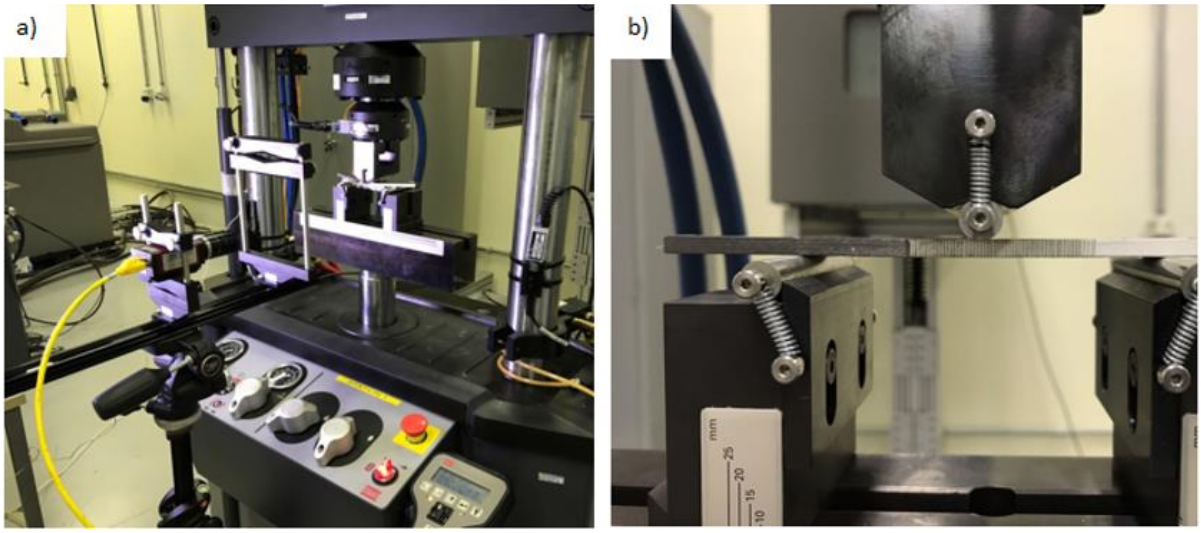

Figure 3: Fatigue Mode II test: a) 3-ENF test setup and b) Sample details.

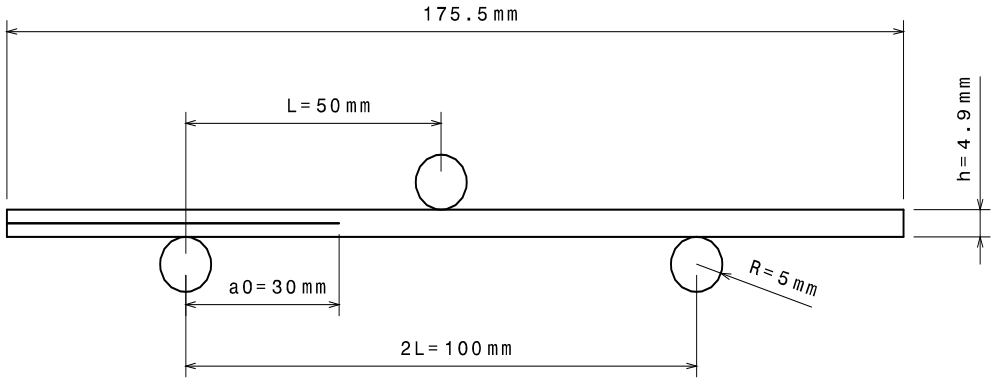

Figure 4: 3ENF specimen, fixture and Dimensions.

The maximum cyclic displacement has been calculated based on Eq.(5).

$$\frac{\delta_{\max}{}^2}{\left[\delta_{cr}\right]_{av}^2} = \frac{G_{IIMax}}{G_{IIc}} \tag{5}$$

where G_{IImax} is being calculated using Eq.(6) (Donadon and Faria, 2016).

$$G_{IIMax} = \frac{3P_c{}^2 a_0{}^2}{8BEI} \tag{6}$$

where

$$I = \frac{Bh^3}{12} \tag{7}$$

where h is sample thickness.

3. RESULTS AND DISCUSSION

3.1 Mode I Fatigue Tests

An experimental campaign of Mode I fatigue tests is being carried out with a goal of totaling 12 samples. Table 1 shows the values of the G/G_c ratios used, the displacements imputed in the MTS machine, the initial max. load values for N = 1 and finally the G_{Imax} and number of cycles. It should be noted that the values of Δ and $\delta_{critical}$ used in Eq. (1) and Eq. (2) were respectively 20.879 and 3.437 mm, which were obtained from the quasi-static tests (Brito *et al.*, 2016).

Table 1. Test parameters and results obtained for Mode I samples.

CDP	**a_0 [mm]**	**R-Ratio [%]**	**δ_{max} [mm]**	**P_0 [N]**	**G_{Imax} [N/mm]**	**N_f [cycles]**
1	59.22	50.00	2.430	27.057	0.061648	1001500
2	62.16	50.00	2.430	29.159	0.063709	928322
3	61.18	55.00	2.549	28.306	0.065704	749772
4	60.20	55.00	2.549	27.314	0.064136	746000
5	59.22	57.50	2.606	30.007	0.072888	479135
6	57.50	57.50	2.606	28.715	0.071103	437500
7	60.30	60.00	2.662	29.125	0.071377	229020
8	62.16	60.00	2.662	29.915	0.071635	244000
9	59.21	62.50	2.717	30.022	0.076304	34500
Average	60.13					

A plot based on Table 1 is shown in Fig. 5, where a trend line was set to check the behavior of G for each G/G_c ratio in order to determine the G No-Growth. The behavior of the Mode I G-N_f curve was quite similar to observed by other researchers (Al-Khudairi *et al*, 2015; Argüelles, *et al*, 2013; Maillet *et al.*, 2015); and also suggested by the standard ASTM D6115 (2004). The fatigue limit under Mode I (DCB) was found to be 50% of the G_{Ic}, representing an average value of G_{Imax} = 0.06268 N/mm, for 10^6 cycles, that satisfies the condition stipulated by Doker and Marci (1983), better known as the fatigue threshold energy (G_{Th}). It is necessary that no crack growth is observed for the applied load (Pmin <P <Pmax). In addition, it is assumed that if a sample withstands 10^6 cycles without showing crack growth, the threshold value is achieved (Doker and Marci, 1983).

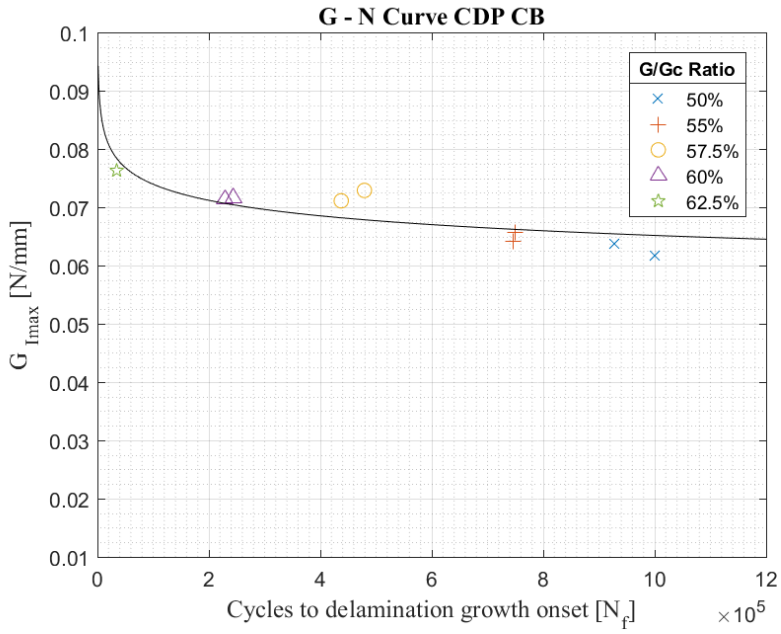

Figure 5: G-N_f curve for Mode I.

3.2 Mode II Fatigue Tests

A typical load-displacement curve obtained from quasi-static test using 3-ENF is shown in Fig. 6, where the critical load and critical displacements are 2383 N and 3.343 mm, respectively. The critical SEER for the material is G_{IIc} = 5.7852 N/mm. This value is in agreement with the value reported by Brito (2016).

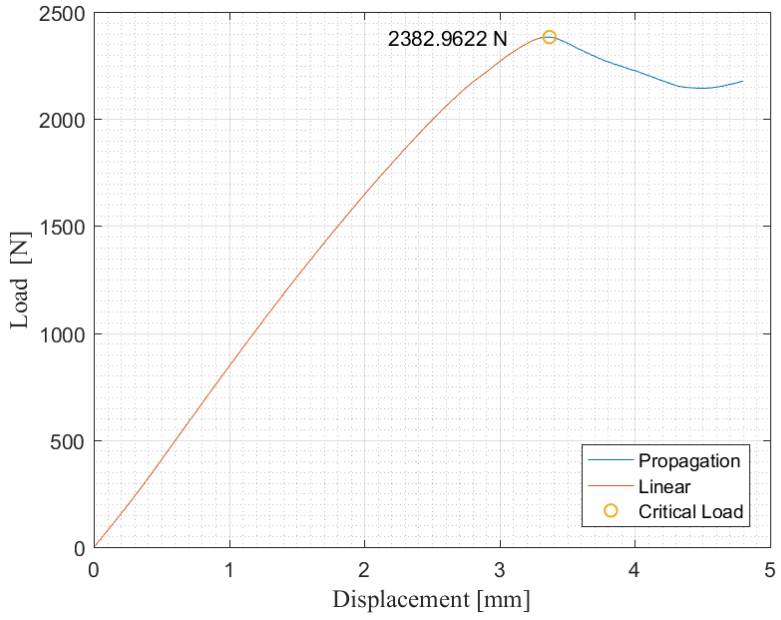

Figure 6: Load-displacement for Mode II.

Table 2 summarizes the values of the initial cracks of the coupons, it is worth mentioning that for Mode II the variable L is not the length of the CDP and becomes the value of the loading span (L = 50 mm) as can see in Fig. 4, in addition it is also presented the values of G_{IImax} and number of cycles found for the tests.

Table 2. Test parameters and results obtained for Mode II samples.

CDP	a [mm]	a_0 [mm]	R-Ratio [%]	δ_{max} [mm]	P_0 [N]	G_{IImax} [N/mm]	N_f [cycles]
1	67.89	30	25.40	2.058	604.80	0.324960	3000
2	65.3	30	4.06	0.823	413.30	0.152508	92000
3	66.54	30	4.06	0.823	353.88	0.110467	84000
4	67.12	30	3.29	0.741	322.26	0.091432	100500
5	68.82	30	3.29	0.741	332.90	0.096982	136500
6	65.81	30	2.60	0.658	299.42	0.076234	1095000
7	64.88	30	2.94	0.658	302.96	0.082363	209500
8	65.64	30	2.94	0.700	305.29	0.082710	263000
9	66.11	30	2.60	0.700	286,56	0.071792	1140500
10	66.21	30	25.40	0.658	606.25	0.323250	2500
11	66.11	30	9.17	1.236	582.63	0.300972	8500
12	66.17	30	9.17	1.236	592.25	0.310354	7500
Average	66.14	30					

A plot based on Table 2 is shown in Fig. 7, where a trend line was adjusted to verify the behavior of G for each G/G_c ratio in order to determine the G No-Growth. The fatigue limit under Mode II (3-ENF) was found to be 2.60 % of the G_{IIc}, representing an average value of G_{IImax}= 0.0740 N/mm for 10^6 cycles, so that is the threshold energy value for Mode II. The behavior of the G-N curve for Mode II was similar to that observed in Mode I, and similar to what found by Hojo *et al.* (2006) and O'Brien *et al.* (2010). Hojo *et al.* (2006) carried out the study in a unidirectional laminate with $[0^o]_{24}$ layup with a polyimide films of 13 μm in thickness as insert on the midplane, used as a crack starter and they found a $G_{IIMaxTh}$ in order of 0.08 N/mm (80 J/m^2).

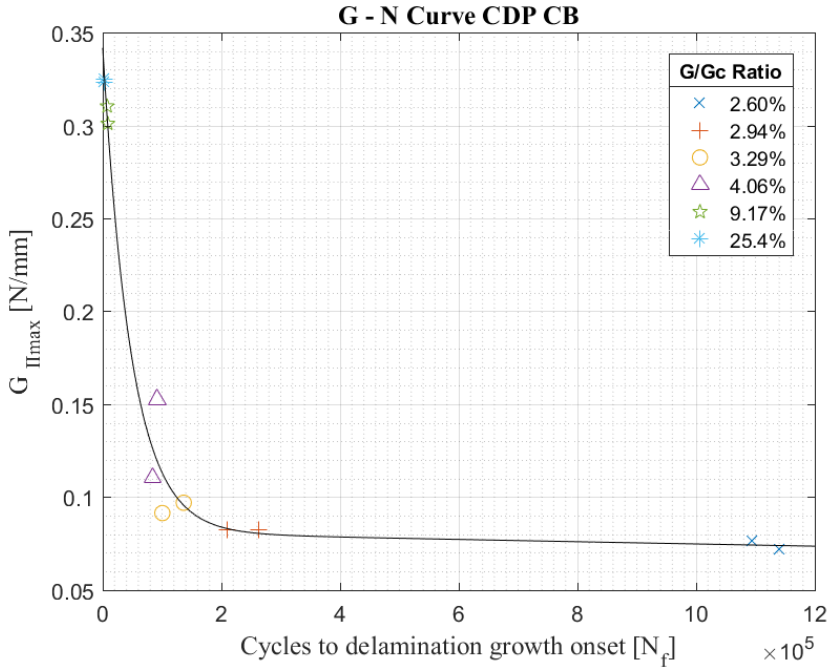

Figure 7: G-N_f curve for Mode II.

An additional plot (Fig. 8) was built with the main objective of comparing the two G-N_f curves obtained and thus comparing the values of G_{max} found for both modes. It can be observed that the values found for G_{max} are higher for Mode II over the whole cycles intervals evaluated.

This is in agreement with what has been found by other researchers (Bradley, 1989; Bonhomme et al., 2009; Hojo et al., 2006) and it has been reported by O'Brien (1997) when the material is more brittle, the value obtained for Mode II

will be greater than Mode I. Brito (2017) reported that this behavior is due to the formation of microcracks which implies that a higher energy is required for the propagation of the damage, a process called microcracking coalescence, resulting in a G_{IImax} greater than a G_{Imax}.

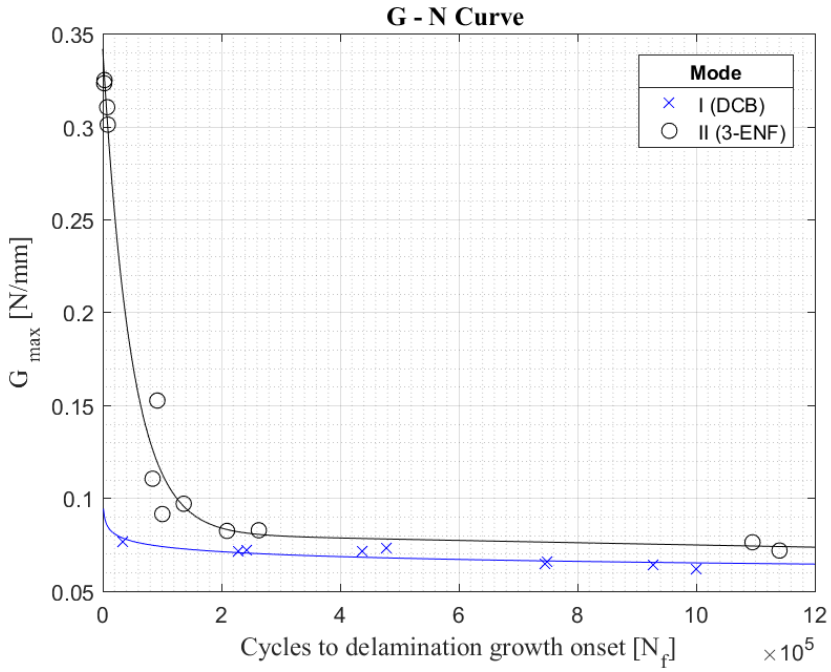

Figure 8: Comparison between G-N_f curve for Mode I and II.

3.3. Fractography analyses

A scanning electron microscope (SEM), model VEGA3 TESCAN®, was used to obtain images to verify if the crack propagated. It is noteworthy that the samples were cut in smaller samples of 65 x 20 x 4.96 mm in order to fit the equipment and then a small layer of gold was deposited through the Q150R Quorum® coating with the objective of improving the visualization of the surface under the microscope.

3.3.1. Mode I

Figure 9.a shows a fractographic image of the region between adhesive and the end of the Teflon and indicate the possible crack growth direction. Figure 9.b provides a higher magnification of the end of the insert, in addition, in the contours of highlighted polyester net there are microcracks that are probably due to the low adhesion of the particles with the adhesive or by the weak interface. In region B is possible to observe the propagation of a microcrack, but it is not possible to confirm that it is related to the fatigue test. It suggests as a cause of micropropagation of the poor positioning of the Teflon, since it is not located in the middle plane of the adhesive. In addition, the Teflon had a contour that may have acted as stress concentrator, since this was the beginning of the propagation or due to the low adhesion with the adhesive or a weaker interface on polyester net. However, it is possible to note the microcrack only in the contour of the polyester net and not in the delaminated sample.

Figure 9.c, it is possible to observe the size of the crack and it can notice its magnitude in the order of the microcrack (~90 μm). Therefore, it is believed that crack propagation did not actually occurred. However, it would be interesting to evaluate another sample with the same G/G_c ratio.

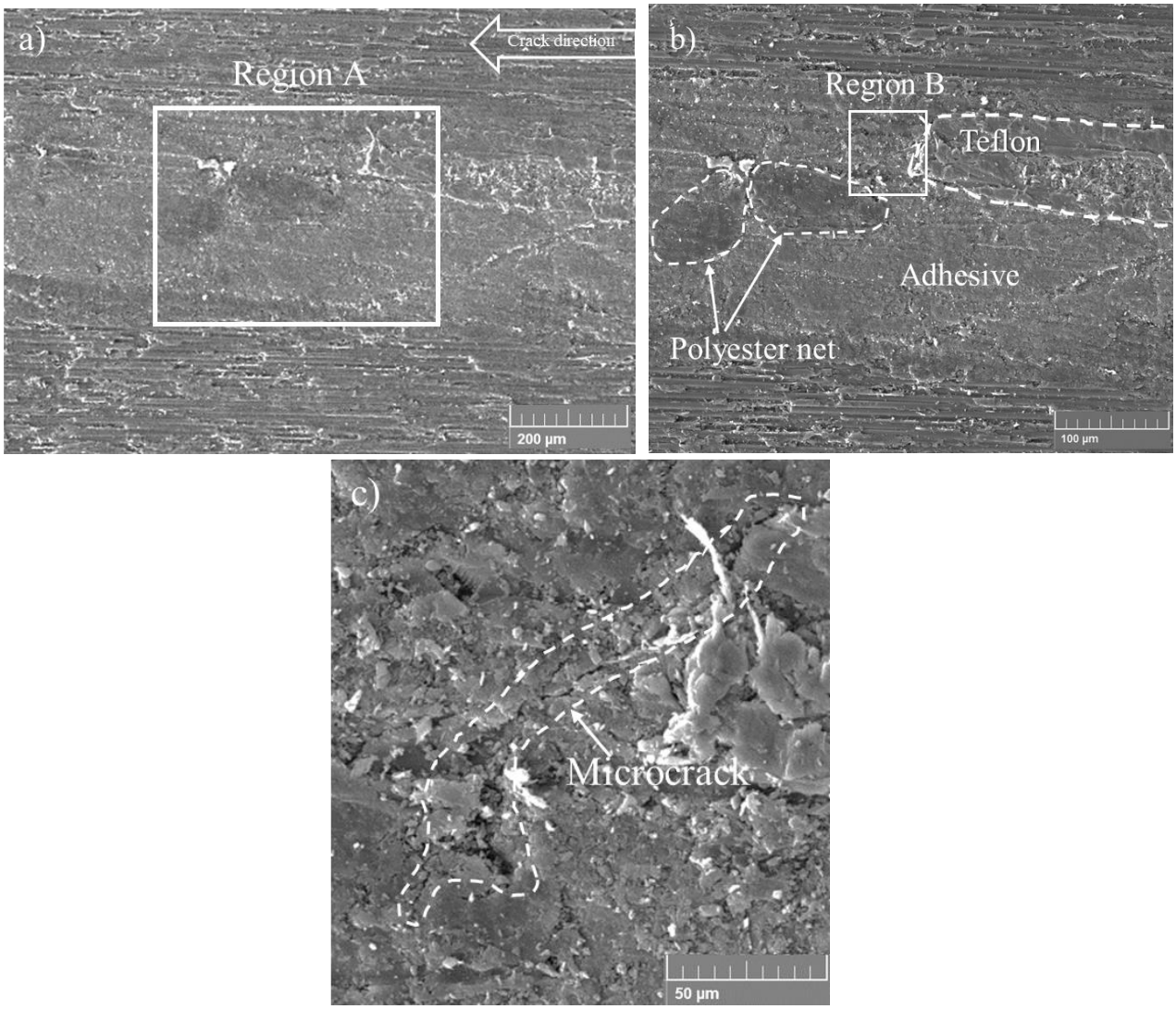

Figure 9: Fracture surface of a co-bonded specimen under Mode I tests a) region between the end of the Teflon insert and the adhesive. b) extension of region A with the indicated areas. c) extension of region B, microcrack indicated. Magnification of 200x, 500x and 1kx, respectively.

3.3.2. Mode II

As can be observed in Fig.10.b, it is noted that no propagation occurred in the sample due to the high ductility of the adhesive or the mesh carrier, which acts as a thickness controller of the adhesive layer, since both can act as an obstacle to the crack front at the beginning of the adhesive. In addition, the elliptical suggests the beginning of a propagation, however the energy supplied was not enough for crack propagation.

Another important point to be observed in Fig.10.b is the propagation around the Teflon and other propagation around the resin pocket, both indicated by arrows in the figure. The authors observed that the crack did not propagate towards the adhesive because of the difference in the physical properties of the two materials, as the resin pocket is stiffer than the adhesive.

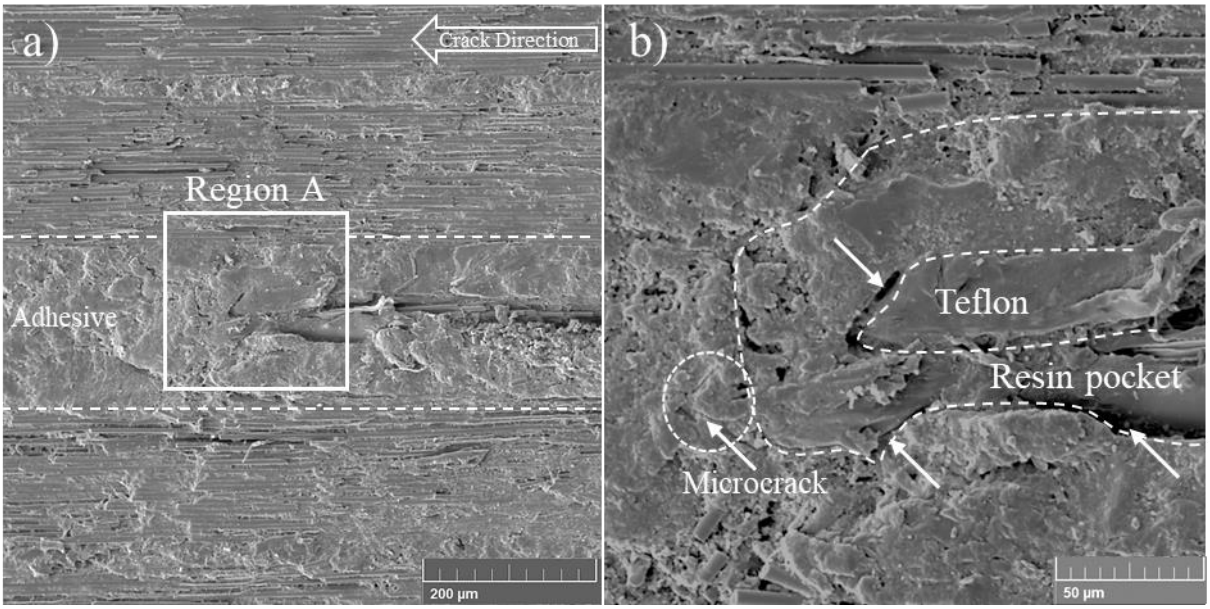

Figure 10: Fracture surface of a co-bonded specimen under Mode II tests a) region between the end of the Teflon insert and the adhesive. b) extension of region A with the indicated areas. Magnification of 200x and 1kx.

4. CONCLUSIONS

The results of the study showed that the values of G_{max} for Mode II are higher than Mode I. Both curves presented similar behavior in terms of G-N_f curve shape as compared with results reported in the open literature. The fatigue threshold values found for Mode I is 0.0627 N/mm and for Mode II is 0.0740 N/mm, both tests ended with 10^6 cycles. In addition, images obtained by S.E.M., it was verified that, for the values of G no-growth found experimentally, the test specimens did not present delamination of the material, that is, the propagation of cracks did not occur.

5. ACKNOWLEDGEMENTS

This project is partially supported by the CNPq processes 126346/2016-0, 142761/2016-8, 800319/2016-8, 800392/2016-7 and 300893/2015-9, Capes 1543373, FINEP 0114018300, IPT/FIPT 991914T and FAPESP 2015/16733-2. The authors also acknowledge the LEL-IPT, the Laboratory of Aerospace Structures and Laboratory of Materials and Processes at ITA for providing the infrastructure and equipments needed for the development of this work, Dr. Geraldo Mauricio Cândido for in-depth and valuable discussions on the fractography analyses.

6. REFERENCES

Al-Khudairi, O., Hadavinia, H., Waggott, A., Lewis, E., & Little, C., 2015. "Characterising Mode I/Mode II fatigue delamination growth in unidirectional fibre reinforced polymer laminates". *Materials & Design* (1980-2015), 66, 93-102.

American Society for Testing and Materials (ASTM) D6115-97. 6115-97(11), 2004. "Standard test method for Mode I fatigue delamination growth onset of unidirectional fiber-reinforced polymer matrix composites". Annual book of ASTM standards, 15.

American Society for Testing and Materials (ASTM) Standard. D7905/d7905m14, 2014. "Standard Test Method for Determination of the Mode II Interlaminar Fracture Toughness of Unidirectional Fiber-Reinforced Polymer Matrix Composites".

Argüelles, A., Coronado, P., Canteli, A. F., Viña, J., & Bonhomme, J., 2013. "Using a statistical Model for the analysis of the influence of the type of matrix carbon–epoxy composites on the fatigue delamination under Modes I and II of fracture". *International Journal of Fatigue*, 56, 54-59.

Bonhomme, J., Argüelles, A., Vina, J., & Vina, I., 2009." Fractography and failure mechanisms in static Mode I and Mode II delamination testing of unidirectional carbon reinforced composites". *Polymer Testing*, 28(6), 612-617.

Bradley, W. L., 1989. "Understanding the translation of neat resin toughness into delamination toughness in composites". *In Key Engineering Materials* (Vol. 37, pp. 161-198). Trans Tech Publications.

Brito, C. B. G., Contini, R. C. M. S., Gouvêa R. F., de Oliveira, A. S. Arbelo, M. A. Donadon, M. V., 2016. "Mode I interlaminar fracture toughness analysis of co-bonded and secondary bonding carbon fiber reinforced composites

joints". *Anais do 22º CBECIMAT - Congresso Brasileiro de Engenharia e Ciência dos Materiais*, Natal, Rio Grande do Norte, Brasil.

Brito, C. B. G., Contini, R. C. M. S., Gouvêa R. F., de Oliveira, A. S. Arbelo, M. A. Donadon, M. V. and Leal, T. P. F. G., 2016. "Interlaminar fracture toughness analysis of co-bonded and secudarily bonded adhesive joints in carbon composites under Mode ii tests." *Anais do XV Brazil MRS Meeting – SBPMat*, Campinas, SP, 2016, Brazil.

Brito, C. B.G., 2017. *Hygrothermal effects on interlaminar fracture toughness of composite joints.* Master dissertation, Instituto tecnológio de aeronáutica – ITA- São José dos Campos, Brazil.

Carreras, L., Renart, J., Turon, A., Costa, J., Essa, Y., & de la Escalera, F. M., 2017. "An efficient methodology for the experimental characterization of Mode II delamination growth under fatigue loading". *International Journal of Fatigue*, 95, 185-193.

Davidson, B. D., Sun, X., & Vinciquerra, A. J., 2007. "Influences of friction, geometric nonlinearities, and fixture compliance on experimentally observed toughnesses from three and four-point bend end-notched flexure tests". *Journal of composite materials*, 41(10), 1177-1196.

Döker, H., & Marci, G., 1983. "Threshold range and opening stress intensity factor in fatigue". *International journal of fatigue*, 5(4), 187-191.

Donadon, M.V. and Faria, A., 2016. "Analysis and design of composite structures - Fracture mechanics applied to composite laminates" - *Notas de aula MP-206*, volume 6. ITA, 2016.

Hojo, M., Ando, T., Tanaka, M., Adachi, T., Ochiai, S., & Endo, Y., 2006. "Modes I and II interlaminar fracture toughness and fatigue delamination of CF/epoxy laminates with self-same epoxy interleaf". *International Journal of Fatigue*, 28(10), 1154-1165.

Loh, W. K., Crocombe, A. D., Wahab, M. A., & Ashcroft, I. A., 2002. "Environmental degradation of the interfacial fracture energy in an adhesively bonded joint*". Engineering fracture mechanics*, 69(18), 2113-2128.

Maillet, I., Michel, L., Souric, F., & Gourinat, Y., 2015. "Mode II fatigue delamination growth characterization of a carbon/epoxy laminate at high frequency under vibration loading". *Engineering Fracture Mechanics*, 149, 298-312.

Odagiri, N., Kishi, H., & Yamashita, M., 1996. "Development of TORAYCA prepreg P2302 carbon fiber reinforced plastic for aircraft primary structural materials". *Advanced Composite Materials*, 5(3), 249-254.

O'Brien, T. K., 1998. "Composite Interlaminar Shear Fracture Toughness, G IIc: Shear Measurement or Sheer Myth?". *In Composite Materials: Fatigue and Fracture*: 7th Volume. ASTM International.

O'Brien, T. K., Johnston, W. M., & Toland, G. J., 2010. "Mode II interlaminar fracture toughness and fatigue characterization of a graphite epoxy composite material".

Sarrado, C., Turon, A., Costa, J., & Renart, J., 2016. "On the validity of linear elastic fracture mechanics methods to measure the fracture toughness of adhesive joints". *International Journal of Solids and Structures*, 81, 110-116.

Sun, X., & Davidson, B. D., 2006. "Numerical evaluation of the effects of friction and geometric nonlinearities on the energy release rate in three-and four-point bend end-notched flexure tests". *Engineering fracture mechanics*, 73(10), 1343-1361.

7. RESPONSIBILITY NOTICE

The authors are the only responsible for the printed material included in this paper.